Title: A non-invasive, 3D, dynamic MRI method for measuring muscle moment arms in vivo: demonstration in the human ankle joint and Achilles tendon.

Authors: EC Clarke[1,2] (PhD, BE, BSc), JH Martin[1,2] (MEngRes, BE), AG d'Entremont[3,4] (PhD, MASc, BE), MG Pandy[5] (PhD, MEngSc, BE), DR Wilson[4] (DPhil, BEng), RD Herbert[6,7] (PhD, MAppSc, BAppSc)

1. Sydney Medical School, The University of Sydney, Sydney, Australia
2. The Kolling Institute of Medical Research, Sydney, Australia
3. Mechanical Engineering, University of British Columbia, Vancouver, Canada
4. Department of Orthopaedics and Centre for Hip Health and Mobility, University of British Columbia and Vancouver Coastal Health Research Institute, Vancouver, Canada
5. Mechanical Engineering, University of Melbourne, Melbourne, Australia
6. Neuroscience Research Australia, Sydney, Australia
7. The University of New South Wales, Sydney, Australia

Correspondence:

Dr Elizabeth Clarke

Murray Maxwell Biomechanics Lab, Level 10, Kolling Building 6

Royal North Shore Hospital, St Leonards, NSW, 2065, AUSTRALIA

Ph: +61-2-9926-4821

Fax: +61-2-9926-5266

Email: elizabeth.clarke@sydney.edu.au

Abstract: 263 words, Manuscript: 3292 words, Tables: 0, Figures: 7

Abstract

Muscle moment arms are used widely in biomechanical analyses. Often they are measured in 2D or at a series of static joint positions. In the present study we demonstrate a simple MRI method for measuring muscle moment arms dynamically in 3D from a single range-of-motion cycle. We demonstrate this method in the Achilles tendon for comparison with other methods, and validate the method using a custom apparatus. The method involves registration of high-resolution joint geometry from MRI scans of the stationary joint with low-resolution geometries from ultrafast MRI scans of the slowly moving joint. Tibio-talar helical axes and 3D Achilles tendon moment arms were calculated throughout passive rotation for 10 adult subjects, and compared with recently published data. A simple validation was conducted by comparing MRI measurements with direct physical measurements made on a phantom. The moment arms measured using our method and others were similar and there was good agreement between physical measurements (mean 41.0 mm) and MRI measurements (mean 42.6 mm) made on the phantom. This new method can accurately measure muscle moment arms from a single range-of-motion cycle without the need to control rotation rate or gate the scanning. Supplementary data includes custom software to assist implementation.

Keywords: Biomechanics; muscle; MRI; muscle moment arm; tendon

Introduction

Muscle moment arms are used widely in biomechanics to relate joint torques and muscle forces, and to estimate changes in muscle length that accompany changes in joint angle. Some examples include the use of muscle moment arms to determine changes in the length of muscles of patients with muscle contractures [1], assessment of changes in muscle stiffness from joint torque measurements [2,3], or development of subject-specific musculoskeletal models [4,5]. These are applications that often involve dynamic joint motion, so ideally the methods used to measure muscle moment arms for dynamic applications would be non-invasive, simple, and obtained from a moving joint. The measurement should be of the true 3D length of the moment arm [6], not the length of the moment arm projected onto an anatomical plane, and it should be given as a continuous function of joint angle, not just at one angle or a small number of discrete joint angles. In some settings (e.g. clinical) it may be desirable for the method to be quick and involve as little joint movement as possible.

Muscle moment arms can be determined in two ways. The ‘geometric method’ involves measuring the distance from the joint axis to the muscle-tendon line-of-action whereas the ‘tendon excursion method’ involves determining the ratio of tendon excursion to joint rotation [7]. A requirement of the tendon excursion method is that the tendon must not be stretched during the joint rotation. The tendon strain seen in vivo as the joint rotates can be circumvented by cutting the tendon so that it can be artificially subjected to constant load during the joint rotation, but it is not possible to cut tendons of healthy human muscles so this approach is best suited to animal muscles or human cadavers. The geometric method obviates the need to cut the tendon, so is better suited for in vivo determination of human muscle moment arms. Imaging technologies can be used to determine the location of the joint axis and muscle-tendon line-of-action.

The simplest methods for geometric measurement of muscle moment arms capture anatomical images of the joint and muscle-tendon unit in a single plane at a few static joint positions. The images are used to calculate two-dimensional centres of rotation between consecutive joint positions, and to measure the distance from each centre of rotation to the muscle-tendon line-of-action in the same plane [8]. A study by Rugg et al demonstrated that Achilles tendon moment arms were only minimally affected when using a fixed versus moving centre of rotation [9]; however, that study was performed using two-dimensional MRI scanning of the ankle joint in sequential stationary postures. Two-dimensional methods may be subject to errors in locating the joint axis because most joints do not behave as planar mechanisms. More recent studies have used three-dimensional imaging techniques to determine the 3D distance between the joint axis and the muscle-tendon line-of-action [6,10-12], and a recent study by Hashizume et al [6] demonstrated that measurements from 2D MRI scans significantly overestimate the Achilles tendon moment arm compared to measurements from 3D MRI scans. While three-dimensional, these methods still involve static positioning of the joint at a small number of joint angles. The interest is often in the moment arm under dynamic conditions (e.g. for dynamic musculoskeletal models or joint dynamometry), and joint axes have been demonstrated to behave differently under static and dynamic conditions [13].

A major technical advance was the use of cine phase-contrast MRI to obtain non-invasive geometric measures of joint helical axes and muscle moment arms in three dimensions under dynamic conditions [14,15]. The technique uses cyclical joint rotation and analysis of velocity encoded data to define the joint helical axes and calculate muscle moment arms. To our knowledge that is the only previously published non-invasive geometric technique that has been used to measure three-dimensional muscle moment arms under dynamic conditions (at the knee and ankle), and therefore as a near-continuous function of joint angle.

Our objective was to develop and validate a non-invasive method to measure 3D dynamic muscle moment arms that could be performed using a single joint rotation cycle, has the potential to be used under either active or passive muscle conditions, and does not require control of joint angular velocity or MRI gating.

Materials and Methods

Participants: Participants were 10 healthy adults (5 men, 5 women) with a mean age of 29 years (range 22-48 years). Healthy subjects were used for ease of comparison with other published methods. All subjects gave written informed consent to participate. The methods were approved by the Human Research Ethics Committee of the University of New South Wales.

MRI scanning: Participants were positioned prone in a 3T MRI scanner (Phillips Achieva, Netherlands) with flexible surface coils strapped to the ankle, and with the foot strapped to a custom jig that allowed an operator to passively rotate the ankle from outside the scanner bore. The thigh and hips were supported on cushions with the knee flexed between 5 and 10 degrees. The relaxed ankle was passively rotated by one of the investigators.

A method for tracking joint position [16,17] was extended to the calculation of muscle moment arms. A key feature of the method is optimised registration (co-localisation) of high-resolution static bone geometries with lower-resolution bone geometries captured using an ultrafast scanning method while the joint is slowly rotated. The coordinates describing the location of the registered geometries were used to reconstruct 3D dynamic joint rotation.

The scanning protocol included one high-resolution 'static' scan of the stationary joint (3D T1-weighted FSE, 4.7 minutes, flip angle 90°, matrix 320×320, FOV 160×160mm, TR/TE = 355.76/16.68ms, slice thickness 1mm) (Figure 1A) followed by a series of low-resolution 'dynamic' scans obtained while the joint was slowly rotated through its range of motion (ultrafast (turbo) gradient echo, 104 seconds, 40 dynamics (phases), 8 slices (sagittal), flip angle 10°, matrix 320×320, FOV 320×320mm, TR/TE = 2.731/1.34ms, slice thickness 4mm, slice gap 0.4-3.0mm, depending on joint size) (Figures 1B-C). The orientation of and gap between the 8 slices across the joint should be subject- and joint-specific; here the slice orientation was aligned with the plane of the Achilles tendon from a coronal view, and the slice gap was adjusted to capture 4-5 slices across the Achilles tendon (see Discussion). The current study used 40 repetitions or time-phases for 1-2 cycles of joint rotation (i.e., 10-20 frames each of joint flexion and extension), which required a total scan time of less than 2 minutes. Dynamic scan data were displayed as 8 ‘movies’ of the rotating joint, one for each of the 8 slices (see supplementary material). The ankle angle for each phase was measured from a single mid-sagittal slice as the angle between the anterior surface of the tibia and the base of the heel on the footplate.

Segmentation: A custom Matlab program (see supplementary material) was used to manually segment the tibia, talus and calcaneus on each slice from the single high-resolution static scan. This produced a dense three-dimensional point-cloud representation of the bone surfaces (Figure 2A). The same program was used to segment the tibia, talus, calcaneus and Achilles tendon for each image in each of the 8 slices generated by the dynamic scans. This produced low-density point-cloud geometries of the rotating bones and tendon (Figure 2B-C and supplementary material).

Registration: The rigid body motion of each segmented bone was reconstructed by registering the high-resolution bone models from the static scan with the low-resolution models from the dynamic scan using a custom Matlab program (see supplementary material). Registration was performed at each joint position using an Iterative Closest Point (ICP) algorithm [18,19]. The particular implementation of the ICP algorithm is stable against mis-registration that could arise when a portion of either model is missing, or when the points in one model lie beyond the bound covered by the other (e.g. when static and dynamic scans have different fields of view of the joint, such as the tibia model in Figure 2C). Corresponding point pairs were rejected if the location of the points differed by >10mm. A sensitivity analysis determined that varying this threshold from 5-15mm had a negligible impact on the quality of the registration. The registration algorithms returned tibio-talar rotation and translation matrices for each instant in time, which were used in the finite helical axis.

Finite helical axis calculation: The tibio-talar joint was used in this study as it is the primary joint responsible for plantarflexion and dorsiflexion of the ankle. Therefore, the helical axis was defined by motion of the talus with respect to the tibia (calculated using a custom Matlab program; see supplementary material). This information can be derived from the standard equation for rigid-body motion, which was used to describe the relative motion of any point on the talus with respect to the tibial reference frame. The use of rigid-body transformation to calculate the helical axis has been well described previously [20].

Muscle moment arm calculation: For each joint angle, midlines were fit between the anterior and posterior tendon segmentations for each sagittal slice; together these midlines defined a surface through the middle of the tendon (Figure 3A-B). The midline of this surface defined the three-dimensional line-of-action through the tendon for each joint angle (Figure 3B). The lines-of-action for all joint angles were stacked together and manually trimmed proximally and distally to a 50mm straight portion, to ensure that the same tendon portions were used for all joint angles (Figure 3C; also see Discussion). The muscle moment arm for each ankle angle was determined as the length of the mutual perpendicular between the joint axis and the tendon line-of-action.

Validation: We developed the custom apparatus shown in Figure 4A-B to validate the MRI method for measuring muscle moment arms. To mimic the bones in a joint, the apparatus uses a sheep tibia and femur, which was cleaned of all soft tissues and rigidly fixed to sections of PVC tubes using perpendicular wooden skewers (Figure 4). To mimic the tendon, a thin latex tube was made and filled with gelatin then secured to the bone surfaces using cable-ties. One of the PVC tubes containing the bones was fixed rigidly to a stationary base plate and the other was fixed to a handle that allowed an operator to rotate the bone about a fixed axis (a PVC tube filled with gelatin). The tendon surrogate was wrapped over a semi-circular PVC tube so that it could glide over a smooth surface with a known distance from the rotation axis. The bones and gelatin tubes were visible in the MRI scans and the tendon path was a known perpendicular distance from the fixed rotation axis (which was physically measured with Vernier callipers). The MRI scans were performed exactly as described above for the volunteers, with the operator rotating the handle on the apparatus as they would for the participants during the dynamic scans. The two sheep bones and the tendon surrogate were analysed in the same way as they were for the participants for calculation of the moment arm.

The physical distance between the tendon surrogate and the PVC tube axis of rotation was known and this value was compared with the 'moment arm' measured using the MRI method.

Results

The individual muscle moment arm measurements throughout ankle dorsiflexion are shown in Figure 5. At the level of individual participants, there were considerable differences in the moment arm-joint angle relationships; that is, the pattern of change in Achilles tendon moment arm with ankle angle was not consistent across all subjects. The mean moment arm (averaged across all measured angles for all subjects) was 51.5 mm.

The mean Achilles tendon moment arm-joint angle relationships obtained under passive (relaxed) ankle rotation using the current 3D dynamic MRI method are shown alongside measurements of Achilles tendon moment arm from other studies[6,9,15,21,22] in Figure 6.

Figure 7 compares the 'moment arms' measured physically and using the current MRI method from the tendon surrogate of our validation apparatus, at 14 different joint angles. The mean of 14 measurements of the 'moment arm' for the validation apparatus, using the current MRI method and the same analysis methods as described for the human subjects, was 41.0 mm (SD=1.0 mm). The mean and maximum absolute differences between the MRI and physical measurements were 1.8 mm and 2.5 mm.

Discussion

The mean Achilles moment arm-joint angle relationships measured with the current MRI method appear similar to the Achilles moment arm-joint angle relationships reported by others (Figure 6). (The exception is the moment arms reported by Hashizume et al [9], which are smaller). This is despite differences in the scanning methods, subject populations, joint loading (active versus passive muscle contraction) and definitions of joint centre of rotation, ankle angle and tendon line-of-action. While there is considerable variation at an individual level (Figure 5), the similarities in population-level data provide evidence of convergent validity.

The validation study performed here for 14 different joint angles showed mean and maximum errors of 1.8 mm and 2.5 mm respectively. The maximum error in the current study was compared with the mean muscle moment arms for each of the 10 subjects, to gain insight into the likely proportion of error in using this method to measure Achilles tendon moment arms in various subjects. The mean Achilles tendon moment arms for individual subjects ranged from 39.6 mm to 64.1 mm, therefore using the maximum error from the validation study (2.5 mm) equates to an error range of 3.9 % to 6.3 % of the mean Achilles tendon moment arm. The maximum error of 2.5 mm from this validation study was also less than the mean error reported by Hashizume et al [6] in performing Achilles tendon moment arm measurements in 2D as compared with 3D, which implies that the current method is more accurate than 2D measurement of the Achilles tendon moment arm.

The MRI method described in this study has some advantages for measurement of muscle moment arms. First, the current method has the potential to be used with either passive movement or under active muscle contraction and can be used to measure either 2D or 3D muscle moment arms. Importantly, using the current MRI method, kinematic data can be directly tracked from a single joint rotation cycle; it does not require repeated cycles of joint rotation like the method based on cine phase-contrast MRI. Another difference from the cine phase-contrast MRI method is that the current method does not require control of the joint angular velocity, nor does it require gating to synchronise the rotation cycle with image capture. For some researchers, this may simplify implementation. It may also be advantageous when the method is used in clinical populations with joint pain or limited movement.

A technical limitation associated with the geometric method of measuring moment arms (including the current MRI method) concerns identification of the tendon line-of-action. For example, Sheehan [15] defined the line-of-action as extending from the soleus myotendinous junction to the insertion of the Achilles tendon on the calcaneus, and Hashizume et al [6] defined the line-of-action as a straight line passing through the centres of the tendon cross-sections at the proximal insertion site on the soleus and distal insertion site on the calcaneus. Another approach has been to define the line-of-action of the tendon as a straight line through a two-dimensional mid-sagittal image of the tendon [21,23]. It would be possible to employ the same definitions of the Achilles tendon line-of-action with the current method but the latter definition cannot be applied when the tendon is curved. In the current study the reason we measured the tendon line-of-action from a 50 mm straight region of the tendon was because we observed curvature in the distal Achilles tendon of several subjects when the ankle was in a plantarflexed position. (The ankle was passively rotated in the current study, but we confirmed that this curvature was also present when the gastrocnemius was actively contracting.) For tendons whose line-of-action is linear it does not matter which part of the tendon is chosen to define the line-of-action. However, some tendons have curved lines of action, either because they pass over underlying structures such as muscles or bones or because they are held down by a retinaculum. The curved part of the tendon cannot be used to calculate the moment arm of the muscle.

A limitation of the current study is that we did not perform multiple measurements on each subject so we could not assess the repeatability of the method in estimating Achilles tendon moment arms. However, the repeatability and accuracy of this MRI scanning has been assessed previously in studies of patella tracking, which found that variability and registration error were within the range of accuracy of the procedure [16,17]. Another limitation of the method is the low through-plane resolution and the limited number of slices containing tendon. The through-plane resolution was sufficient to define the anterior and posterior surfaces of the tendon (and therefore a midline surface), but did not allow us to define centroids through re-sliced axial cross sections, which would have been ideal. It may be possible, with an appropriate scanning field of view, to use ultrafast MRI scanning to track the three-dimensional locations of the myotendinous junction and calcaneal insertion.

The particular protocol presented here would be particularly useful for measuring moment arms in adults, and for tendons that are relatively wide with respect to their joint. However with some protocol modifications the MRI method itself may also be useful for other tendons and in smaller joints of children. For example, when obtaining measurements from smaller joints and smaller subjects such as children it would be necessary to reduce the slice gap for the dynamic scanning protocol so that the slices span the width of the joint. Also, for measuring moment arms in tendons that are narrow with respect to the joint (e.g. medial or lateral gastrocnemius at the knee) it would be necessary to increase the number of slices for the dynamic scanning protocol so that there are several slices through the tendon and so that the slices span the width of the joint. More slices provide more detailed spatial information for geometry registration, but they do so at the cost of increasing the scanning time per phase. That may be accommodated by slowing the joint motion to maintain joint angle resolution and minimise motion artefact. We found that a minimum of 5 slices was needed to register bone position, but increasing the number of slices beyond 8 produced blurring on the dynamic scans at the rotation speed we used. Acquisition speed could be improved by reducing the field of view. It is most important to select a slice gap that provides sufficient detail of the bones and muscle-tendon units of interest. Another parameter that could be varied is the number of phases (or repetitions): we used 40 phases which provided 10-20 data points per joint rotation from plantarflexion to dorsiflexion. The number of phases could be reduced to reduce total scan time (which might be advantageous if scans were to be obtained from participants while they performed intense muscle contractions or clinical populations with pain), or increased to capture replicates for averaging.

We have presented an MRI method for measuring 3D muscle moment arms while the joint is slowly rotating, and we compared measurements made with this method to direct physical measurements from a surrogate validation apparatus. The method was demonstrated in the human Achilles tendon under passive muscle conditions, but it also has the potential to be applied to other muscles and under active muscle conditions. The method is capable of measuring the muscle moment arm from a single cycle of joint rotation, without the need for controlling angular velocity or (MRI-) gating the rotation cycle. This could make the method particularly suitable for application to clinical populations.

Acknowledgements

EC and RH are supported by NHMRC research fellowships. Funding for this study was provided by a pilot project grant from the Sydney Medical School, University of Sydney and by Canadian Institutes of Health Research Grant #MOP-106680.

References

1. Diong, J. H., Herbert, R. D., Harvey, L. A., Kwah, L. K., Clarke, J. L., Hoang, P. D., et al. Passive mechanical properties of the gastrocnemius after spinal cord injury. Muscle Nerve. 2012. 46: 237-45.
2. Hoang, P. D., Gorman, R. B., Todd, G., Gandevia, S. C., and Herbert, R. D. A new method for measuring passive length-tension properties of human gastrocnemius muscle in vivo. J Biomech. 2005. 38: 1333-41.
3. Hoang, P. D., Herbert, R. D., Todd, G., Gorman, R. B., and Gandevia, S. C. Passive mechanical properties of human gastrocnemius muscle tendon units, muscle fascicles and tendons in vivo. J Exp Biol. 2007. 210: 4159-68.
4. Ackland, D. C., Lin, Y. C., and Pandy, M. G. Sensitivity of model predictions of muscle function to changes in moment arms and muscle-tendon properties: A monte-carlo analysis. J Biomech. 2012. 45: 1463-71.
5. Scheys, L., Van Campenhout, A., Spaepen, A., Suetens, P., and Jonkers, I. Personalized mr-based musculoskeletal models compared to rescaled generic models in the presence of increased femoral anteversion: Effect on hip moment arm lengths. Gait Posture. 2008. 28: 358-65.
6. Hashizume, S., Iwanuma, S., Akagi, R., Kanehisa, H., Kawakami, Y., and Yanai, T. In vivo determination of the achilles tendon moment arm in three-dimensions. J Biomech. 2012. 45: 409-13.
7. Pandy, M. Moment arm of a muscle force. Exercise and Sport Sciences Reviews. 1999. 27: 79-118.
8. Maganaris, C. N. Imaging-based estimates of moment arm length in intact human muscle-tendons. Eur J Appl Physiol. 2004. 91: 130-9.

9. Rugg, S. G., Gregor, R. J., Mandelbaum, B. R., and Chiu, L. In vivo moment arm calculations at the ankle using magnetic resonance imaging (mri). J Biomech. 1990. 23: 495-501.

10. Fowler, N. K., Nicol, A. C., Condon, B., and Hadley, D. Method of determination of three dimensional index finger moment arms and tendon lines of action using high resolution mri scans. J Biomech. 2001. 34: 791-7.

11. Graichen, H., Englmeier, K. H., Reiser, M., and Eckstein, F. An in vivo technique for determining 3d muscular moment arms in different joint positions and during muscular activation - application to the supraspinatus. Clin Biomech (Bristol, Avon). 2001. 16: 389-94.

12. Krevolin, J., Pandy, M., and Pearce, J. Moment arm of the patellar tendon in the human knee. Journal of Biomechanics. 2004. 37: 785-788.

13. d'Entremont, A., Nordmeyer-Massner, J., Bos, C., Wilson, D., and KP, P. Do dynamic-based mr knee kinematics methods produce the same results as static methods? Magnetic Resonance in Medicine. 2012. 69: 1634-44.

14. Sheehan, F. T. The finite helical axis of the knee joint (a non-invasive in vivo study using fast-pc mri). J Biomech. 2007. 40: 1038-47.

15. Sheehan, F. T. The 3d in vivo achilles' tendon moment arm, quantified during active muscle control and compared across sexes. J Biomech. 2012. 45: 225-30.

16. Fellows, R. A., Hill, N. A., Gill, H. S., MacIntyre, N. J., Harrison, M. M., Ellis, R. E., et al. Magnetic resonance imaging for in vivo assessment of three-dimensional patellar tracking. J Biomech. 2005. 38: 1643-52.

17. Fellows, R. A., Hill, N. A., Macintyre, N. J., Harrison, M. M., Ellis, R. E., and Wilson, D. R. Repeatability of a novel technique for in vivo measurement of three-dimensional patellar tracking using magnetic resonance imaging. J Magn Reson Imaging. 2005. 22: 145-53.

18. Rusinkiewicz, S. and Levoy, M. Efficient variants of the icp algorithm. Third International Conference on 3-D Digital Imaging and Modeling, Proceedings. 2001. 145-152.

19. Besl, P. and McKay, N. A method for registration of 3-d shapes. IEEE Transactions on Pattern Analysis and Machine Intelligence. 1992. 14: 239-256.

20. Spoor, C. W. and Veldpaus, F. E. Rigid body motion calculated from spatial co-ordinates of markers. J Biomech. 1980. 13: 391-3.

21. Fath, F., Blazevich, A. J., Waugh, C. M., Miller, S. C., and Korff, T. Direct comparison of in vivo achilles tendon moment arms obtained from ultrasound and mr scans. J Appl Physiol. 2010. 109: 1644-52.

22. Maganaris, C. N., Baltzopoulos, V., and Sargeant, A. J. In vivo measurement-based estimations of the human achilles tendon moment arm. Eur J Appl Physiol. 2000. 83: 363-9.

23. Maganaris, C., Baltzpoulos, V., and Sargeant, A. Changes in achilles tendon moment arm from rest to maximum isometric plantarflexion: In vivo observations in man. Journal of Physiology. 1998. 510: 977-985.

Figure legends

Figure 1. Representative static and dynamic images: (A) one mid-sagittal image from the high-resolution static scan. (B) One mid-sagittal image from the low-resolution dynamic scan during plantarflexion and (C) dorsiflexion.

Figure 2. Registration of high-resolution static geometries with low-resolution dynamic geometries: (A) three-dimensional point-cloud geometries of the tibia (blue), talus (green) and calcaneus (red) constructed by segmenting the high-resolution static scan, (B) three-dimensional point-cloud geometries of the tibia, talus, calcaneus and Achilles tendon constructed by segmenting the bones and tendon from the 8 slices of the low-resolution dynamic scan stack, and (C) registration of the three-dimensional bone geometries shown in A (coloured) with the dynamic slices shown in B (black).

Figure 3. Tendon line-of-action: (A) three-dimensional geometries of the tibia, talus, calcaneus and Achilles tendon at a single joint angle. (B) Schematic of a representative tendon midline surface (grey grid surface) and the accompanying tendon midline (bold black line), for a single joint angle. (C) Stacked tendon midlines for all joint angles segmented for a single subject showing representative proximal and distal trim lines applied to all joint angles.

Figure 4. Validation apparatus: the validation apparatus was constructed to mimic the bones and tendons from a joint but with the ability to physically measure the ‘moment arm’. Gelatin-filled tubing was used to model the tendon and fixed axis of rotation. Dissected animal bones were used to mimic the bones in a human joint: one was fixed stationary to the base plate, and the other rotated about a fixed gelatin-filled PVC tube axis. The tendon surrogate was fastened to the bones using cable ties and glided over another fixed PVC tube axis of larger diameter. The distance from the surrogate tendon to the fixed rotation axis was physically measured from the apparatus for comparison with the MRI method.

Figure 5. Achilles tendon moment arms of individual participants: unscaled Achilles tendon moment arm-joint angle relationships (black symbols) for 10 individual participants. Each participant's data is shown in a separate panel. The differences in the range of ankle joint angles between subjects (i.e., differences in the range of the x-axis) are due to differences in ankle flexibility.

Figure 6. Comparison of moment arms estimated using several 3D MRI methods: the prominent step from low to high moment arm using the current MRI method at an ankle angle of approximately 65 degrees occurred because subjects were tested over different ranges of motion. The current MRI method compares well with other measurements in the literature, despite differences in the methods and subject populations. The data from the current study are mean moment arms for all 10 subjects, measured in 3D while the ankle is being passively rotated. Data from Sheehan are unscaled moment arms measured in 3D under active ankle rotation. Data from Hashizume et al are mean moment arms measured in 3D with the ankle at rest at a range of angles. Data from Fath et al and Maganaris et al are mean moment arms measured in 2D with the ankle relaxed at rest for a range of ankle angles, using a moving centre of rotation method. The data from Rugg et al are mean moment arms measured in 2D with the ankle at rest but under active muscle contraction, using a centre of rotation method.

Figure 7. Measurements from the validation apparatus: the data points are MRI measurements from a single rotation movement of the surrogate validation apparatus and the solid line is the physical measurement of the 'moment arm' from the centre of the rotation axis to the tendon surrogate.

Supplementary material 1. Video file showing 27 dynamic phases for one mid-sagittal slice through a representative ankle. The complete dynamic scan set for this study included 8 slices across the ankle for 40 dynamic phases.

Supplementary material 2. Video file showing registration of the high-resolution static geometries with low-resolution dynamic geometries for 27 dynamic phases.

Supplementary material 3. Link to google code website containing custom Matlab code for segmentation, registration, helical axis and muscle moment arm calculation

Figure

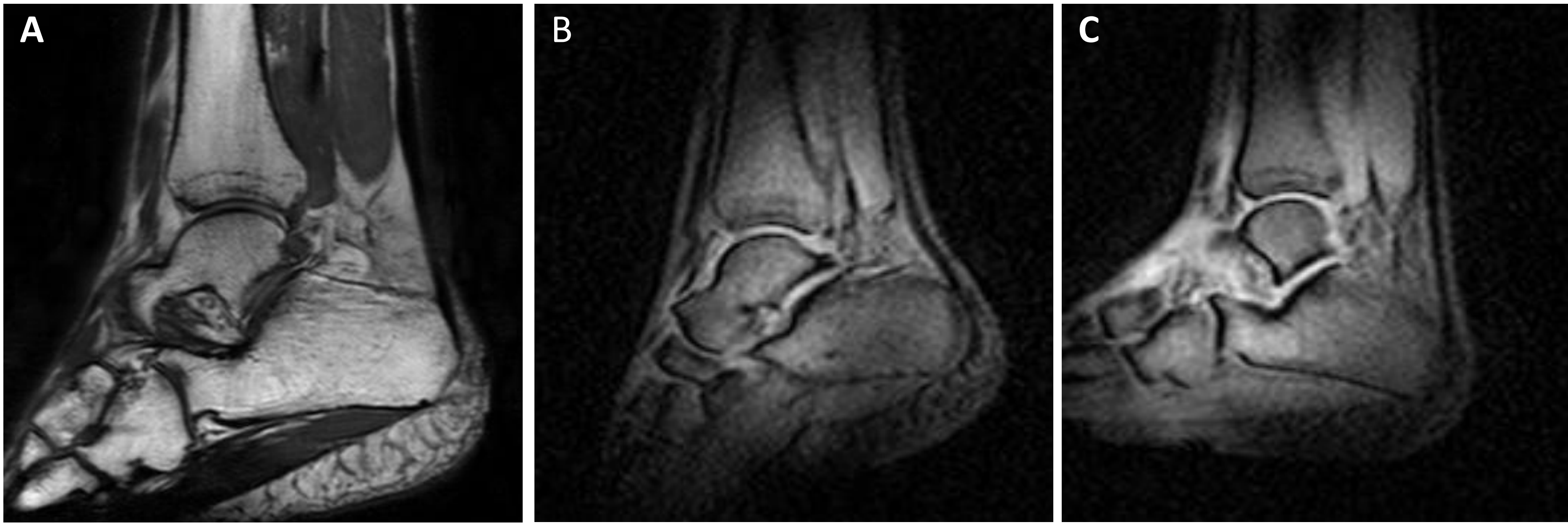

Figure 2

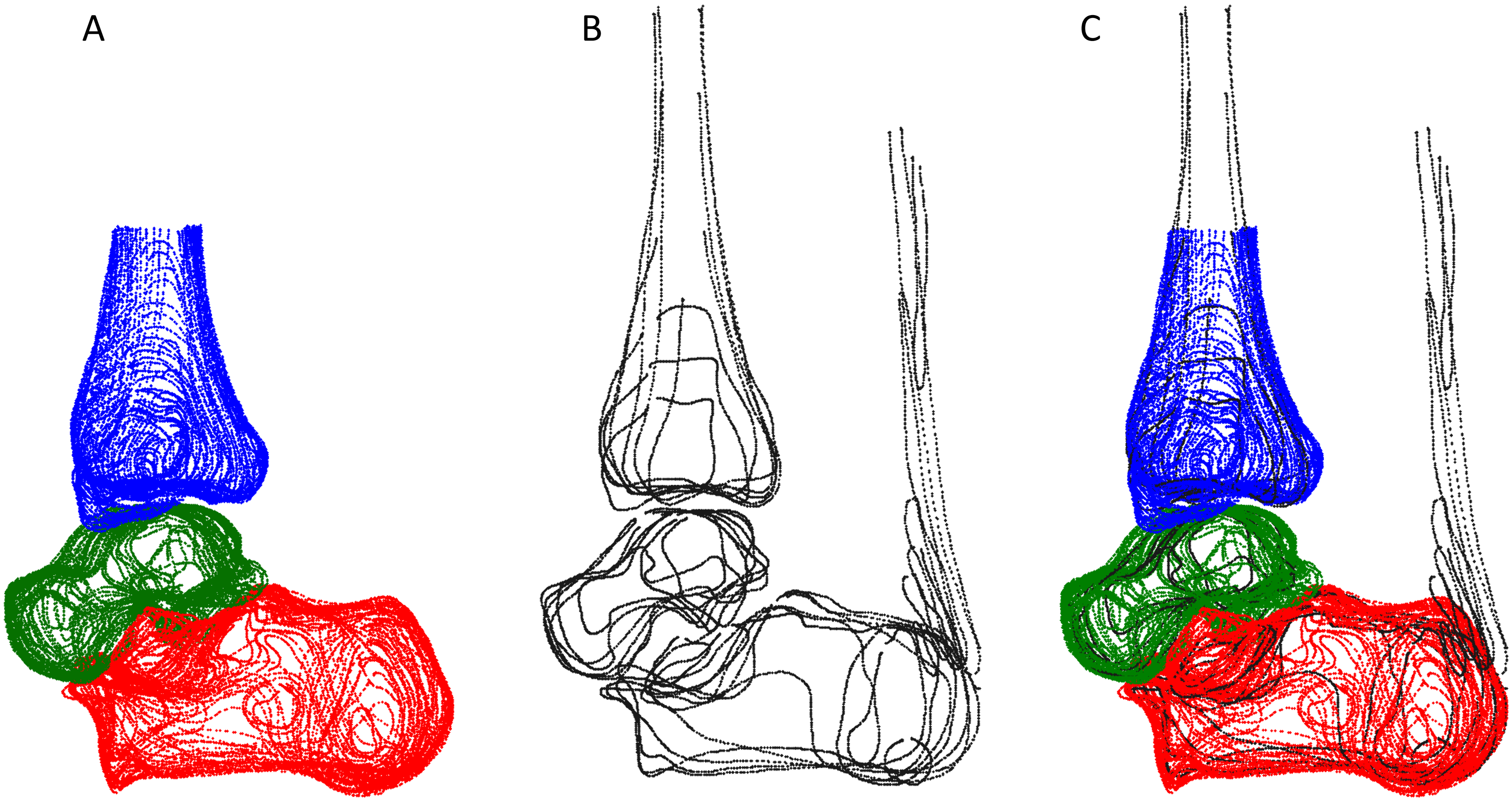

Figure 3

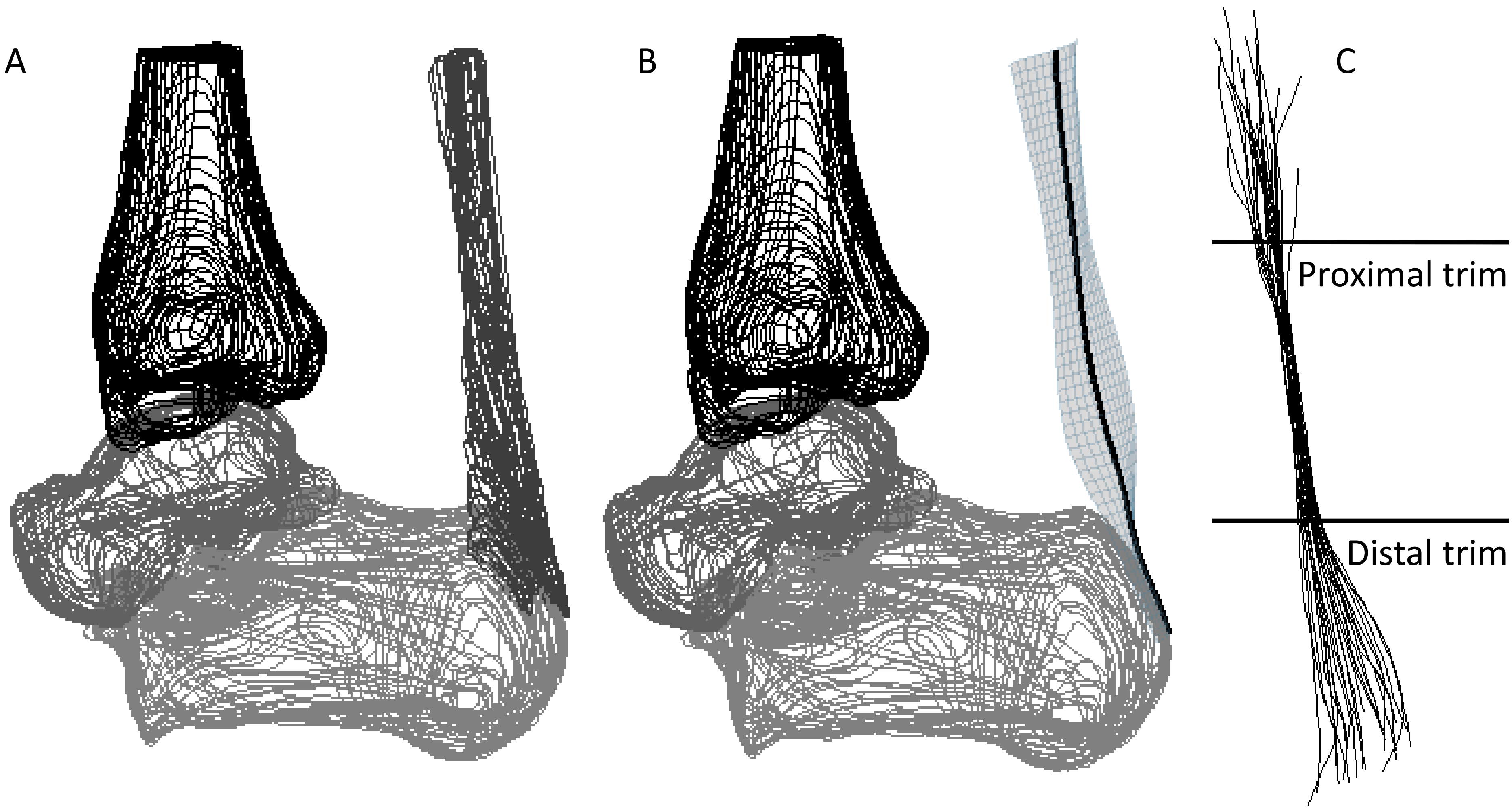

Figure 4A

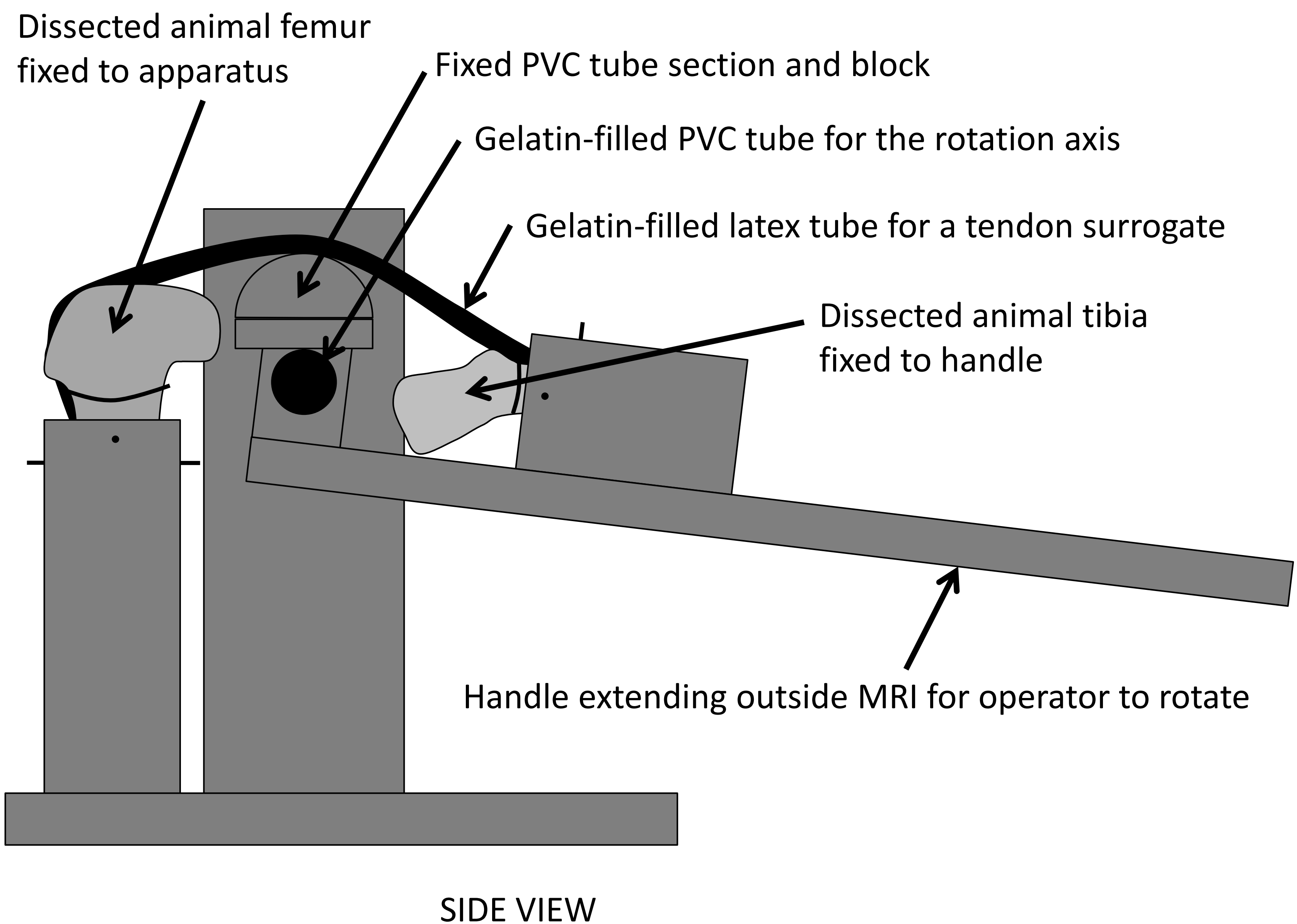
Dissected animal femur fixed to apparatus
Fixed PVC tube section and block
Gelatin-filled PVC tube for the rotation axis
Gelatin-filled latex tube for a tendon surrogate
Dissected animal tibia fixed to handle
Handle extending outside MRI for operator to rotate
SIDE VIEW

Figure 4B

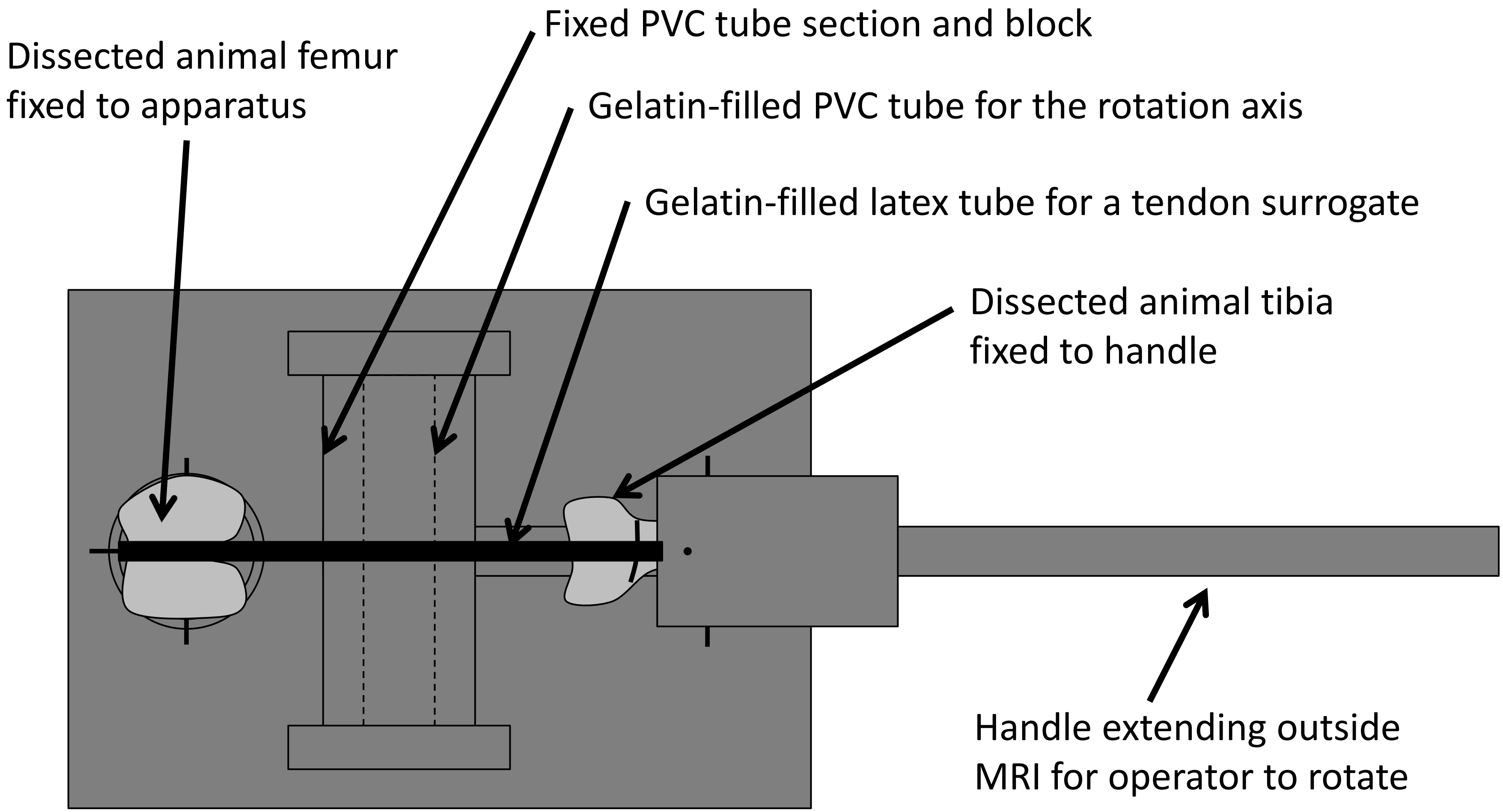

TOP VIEW

Figure 5

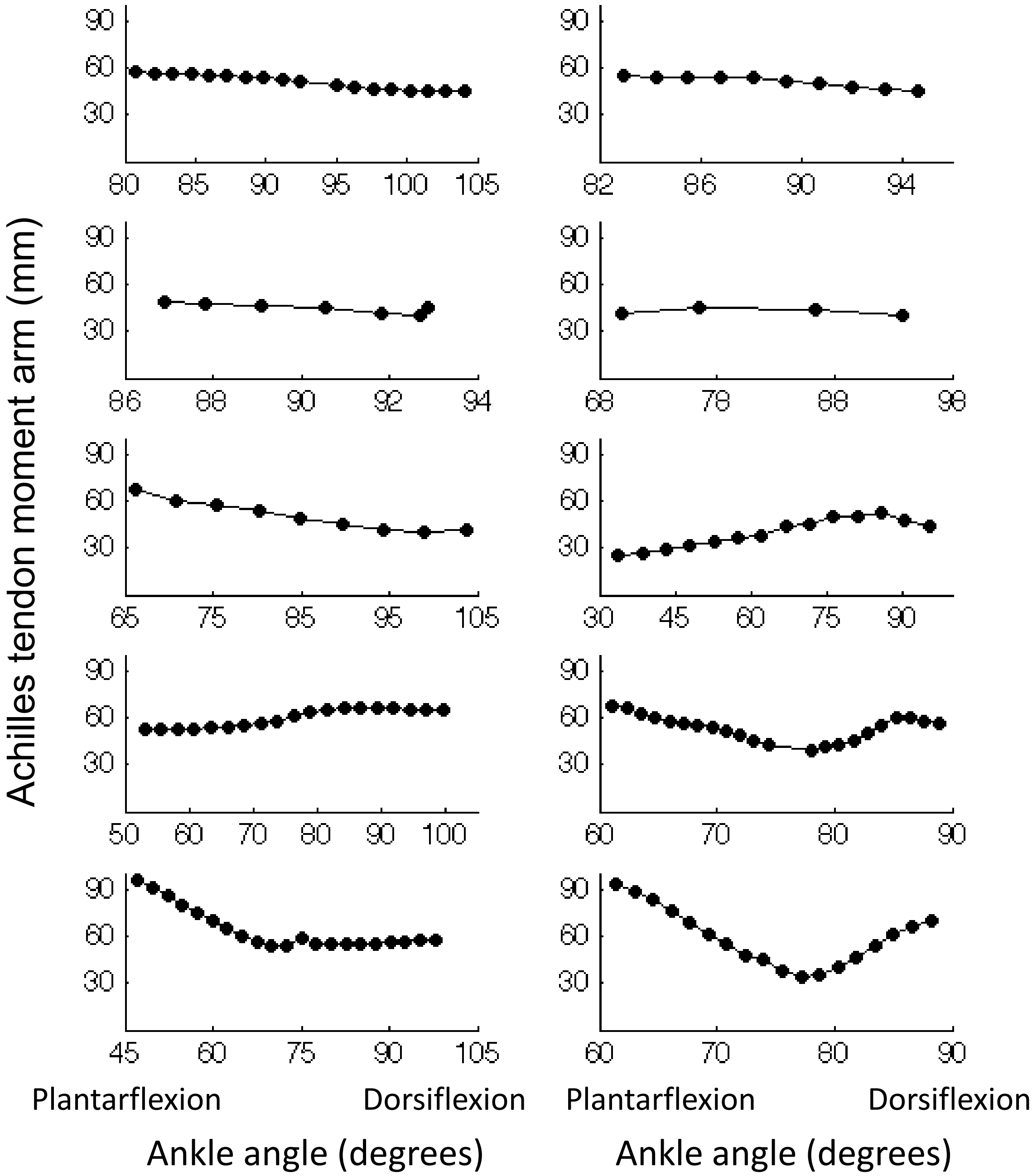

Achilles tendon moment arm (mm)
90
60
30
80 85 90 95 100 105
82 86 90 94
86 88 90 92 94
68 78 88 98
65 75 85 95 105
30 45 60 75 90
50 60 70 80 90 100
60 70 80 90
45 60 75 90 105
60 70 80 90
Plantarflexion
Dorsiflexion
Plantarflexion
Dorsiflexion
Ankle angle (degrees)
Ankle angle (degrees)

Figure 6

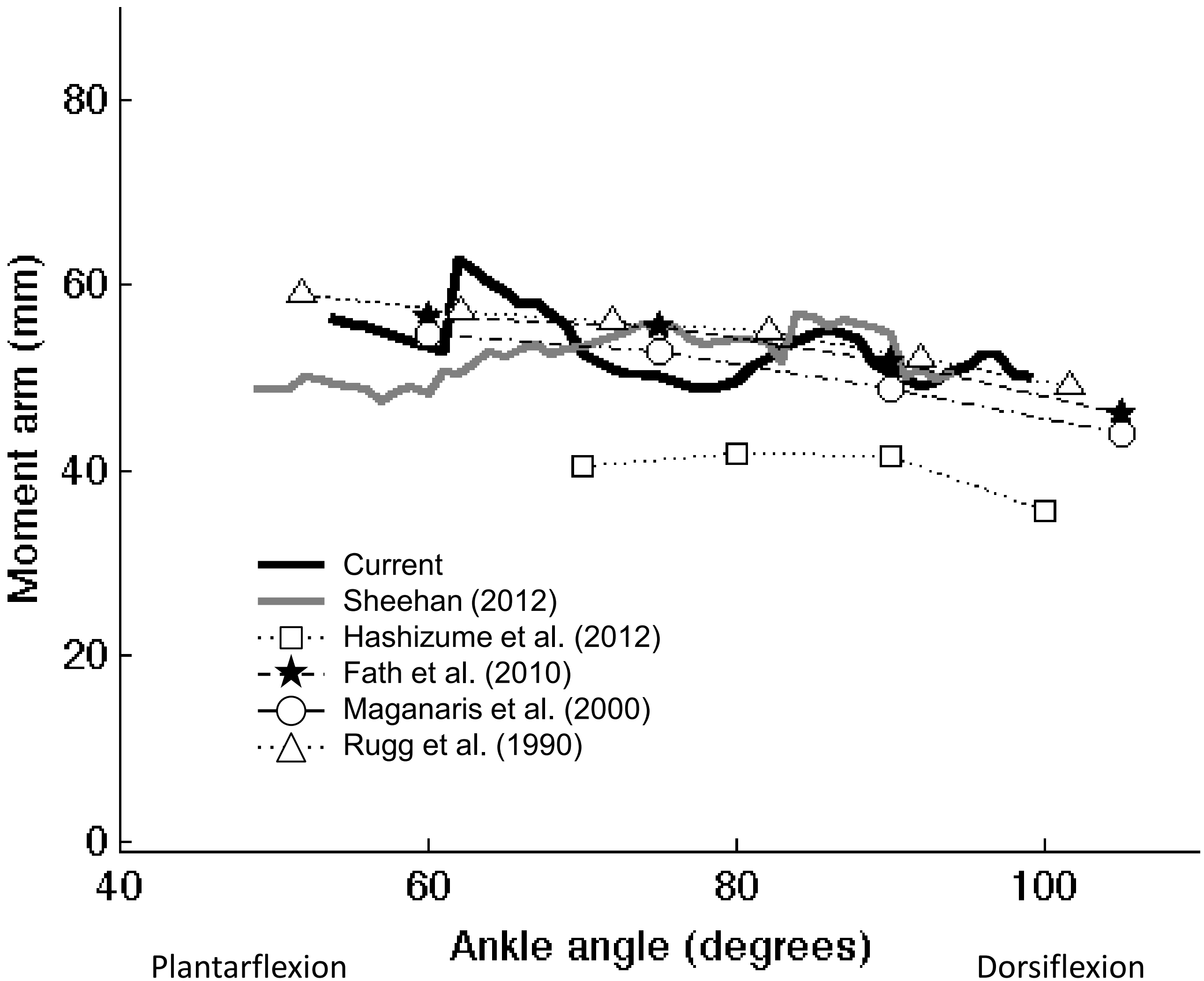

Moment arm (mm)
0
20
40
60
80
40
60
80
100
Ankle angle (degrees)
Plantarflexion
Dorsiflexion
Current
Sheehan (2012)
Hashizume et al. (2012)
Fath et al. (2010)
Maganaris et al. (2000)
Rugg et al. (1990)

Figure 7

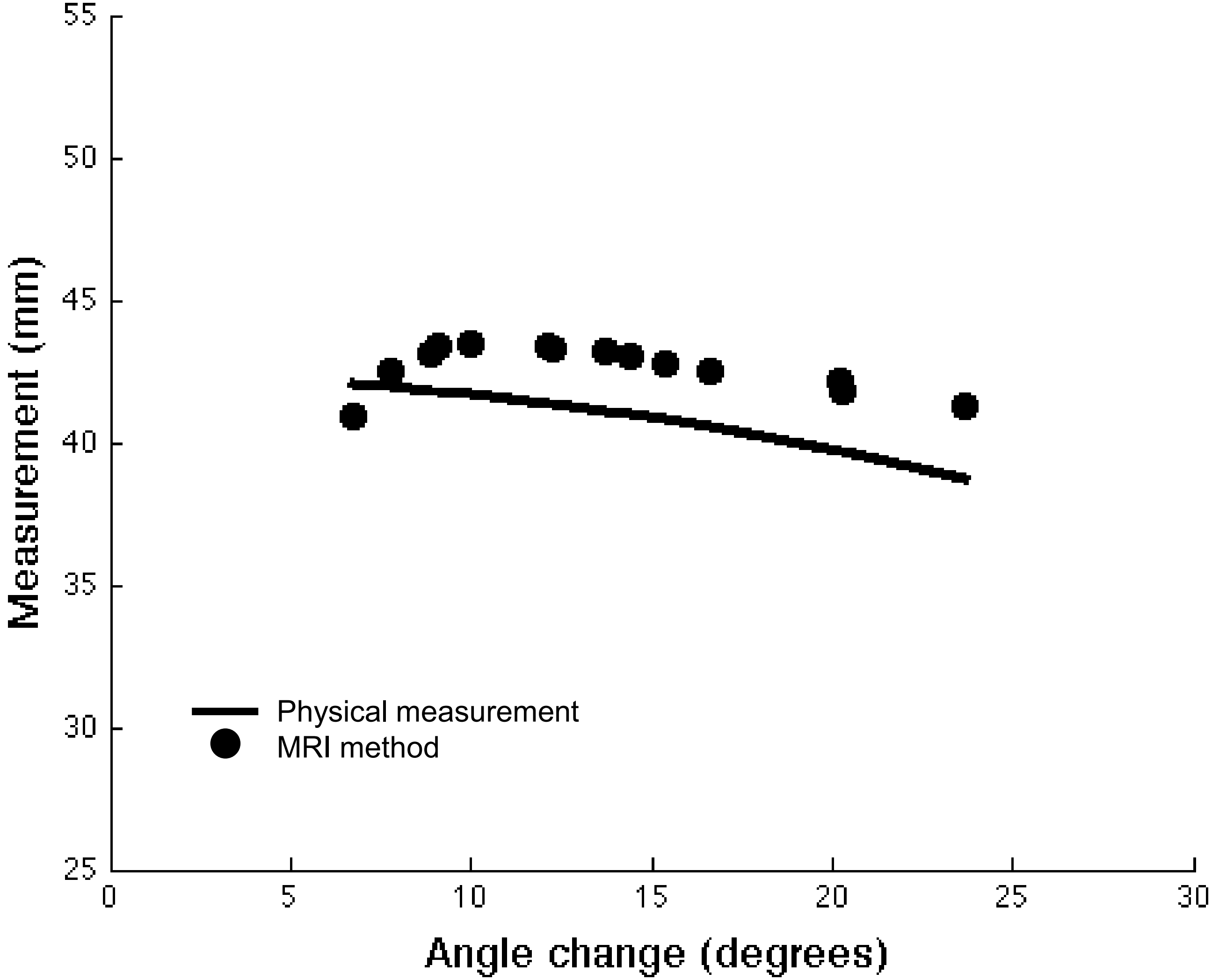

55
50
45
40
35
30
25
0
5
10
15
20
25
30
Measurement (mm)
Angle change (degrees)
Physical measurement
MRI method

Supplementary data 1

Click here to download Supplementary data: SupMaterial_Movie_Figure1.avi

Supplementary data 2

Click here to download Supplementary data: SupMaterial_Movie_Figure2.avi

Supplementary data 3

Click here to download Supplementary data: SupMaterial_3.docx